Supporting Information Appendix for:

The role of forest regrowth in global carbon sink dynamics

Contains

- Supporting Methods
- Supporting Tables S1 to S4
- Supporting Figures S1 to S9
- Supporting Datasets S1 and S2
- Supporting References

Supporting Methods

Confidence intervals on GFAD. We created two additional age map estimates building on the standard version of GFAD (1), representing the lower and upper confidence intervals of forest stand age distribution. In the regions where the stand age distribution was calculated based on forest inventories we applied an age uncertainty of ±40% based on error in age determination reported by the US Forest Service (2). These age uncertainties are reported as a 90% confidence interval, but applying a best fit curve to their age versus uncertainty data finds 95% confidence interval to be almost identical. The estimate of ±40% likely errs on the large side because of error cancellation when aggregated over space. We estimated uncertainty in the tropical regions by propagating the 95% confidence intervals in biomass (3) through the biomass ages curves.

Disturbance during LPJ-GUESS spin-up in GFAD-forced simulations. We calculated a stand-replacing-disturbance return period based on the rate of forest loss in the period 1981-2010 of the GFAD dataset. This was carried out by dividing the total fraction of forest established in each 0.5° grid cell over 1981-2010 by 30 years in order to give a mean annualized forest establishment rate. It was assumed that disturbance rates and establishment rates were equivalent. This mean rate was then converted into a disturbance rotation period by dividing the total forest area fraction in a grid-cell in 2010 by the annual disturbance rate in that grid-cell. We assume that this mean disturbance rotation period per grid-cell is equivalent to the return period at any point within that grid-cell. Return periods were capped at 1000 years and for grid cells with very low forest area or no data, a period of 100 years was assumed. We acknowledge that this assumes current disturbance rates, including forest harvest, are applied in the pre-industrial period, but given that very limited data exists on disturbance rates across biomes, this choice is a substantial improvement over considering a single universal value. The assumption will be particularly valid in the tropical forest, where stand-replacing disturbances are rare events (4, 5). Disturbance events during spin-up were partitioned between fire and "other" disturbances using the LPJ-GUESS fire model (6). For "other" disturbances the disturbed biomass was transferred to litter.

Sensitivity simulations. Additional information on sensitivity set-ups S1 and S2 is as follows:

S1) There is uncertainty regarding the fate of disturbed material, because GFAD gives no information about the type of forest disturbance. In the standard simulation it is assumed that 66% of disturbed material on the remaining land is removed from the ecosystem through harvest or burning. As not all natural disturbances result in wood being removed or burnt, sensitivity simulations were also conducted where this disturbed material remained in the ecosystem. However, as it would be unrealistic to assume that all disturbed material remains in the ecosystem in most forests where humans are active, this sensitivity test was only applied in grid cells defined as wild forest by Ellis et al. (7) (after aggregating to 0.5° from 5 arc minute resolution based on the mode classification).

S2) GFAD gives no information on previous land-use, which may be managed forest, pasture or cropland, rather than the old-growth forest assumed in our standard simulations. The implications of this may be particularly large for soil carbon stocks (8). As croplands provide the most extreme differences in soil carbon compared to forest soils (9, 10), we tested the sensitivity to this assumption by carrying out a simulation where all land was initialized as cropland. Crop type and fertilization rate were prescribed as in Olin et al. (11), extrapolating these following the nearest neighbor rule for grid cells in which no cropland was simulated in that study. Because this sensitivity test would be totally unrealistic in a wild forest, grid cells defined as wild forest by Ellis et al. (7) were simulated using standard settings.

Modelling forced by LUH2. The version of LPJ used here was an update of Sitch et al. (12) which allows to explicitly track fractions of regrowth forest within each grid cell (10-year stand age-classes from 1-100 {1-10 years, 11-20 years, ... , 91-100 years}, 101-150 years, and 150+ years; corresponding to stand age-classes typical of forest inventory data). Among stand age-classes in a grid cell, climate, atmospheric CO_2 concentration and soil texture are similar, whereas resources for plants (e.g., space, light, water) may differ depending on demand; as such, processes related to photosynthesis, plant competition and heterotrophic

respiration are simulated at the level of the age-class. Stand age-classes are created via fire on stands with no history of land-use change, whereas on forest stands with a history of land use change, age-classes are created by fire and via land-use transitions.

LPJ does not model size cohorts within stand age classes, but follows an area-based approach to within-stand dynamics (12). Competitive advantages occur when a plant functional type (PFT) has greater growth efficiency, more positive annual carbon balance, and greater tolerances to heat stress and water availability. Less competitive PFTs undergo reductions in PFT-specific tree densities (i.e. mortality). Explicit competition for light occurs if the total tree foliar projective cover is above 95% of the stand area. In which case, shading mortality is partitioned among PFTs according to the annual allocation to leaf area to maintain a maximum tree foliar projective cover in the stand of 95%.

In LPJ, deforestation results in 100% of heartwood biomass and 50% of sapwood biomass being removed from the ecosystem, with the remaining biomass being transferred to litter pools. Harvest results in 60% of heartwood and sapwood being removed from the ecosystem.

The version of the CABLE model used here incorporates the POP vegetation demographic model which is fully described in Haverd et al. (13, 14). Competition between cohorts in CABLE is governed by self-thinning, as influenced by crowding of crowns, and size-dependent resource limitation constraints (14). CABLE used coefficients for removal of harvested and cleared biomass from the ecosystem following (15).

All three DGVMs simulated transitions due to both forest harvest and land abandonment in the LUH2-forced simulations. LPJ-GUESS tracked these two transition types separately.

Supporting Tables

Table S1. Decadal regrowth forest areas and carbon uptake calculations for regrowth forest under constant forcing.

	TrBE	TrBD	OTr	TeBE	TeBD	NE	ND	MX	Other	Units
1981-1990										
Regrowth area, GFAD	0.88	0.56	0.19	0.37	2.60	6.37	2.39	0.85	0.66	M km^2
Regrowth area, LUH2	1.48	0.47	0.20	0.49	2.49	3.12	1.62	0.70	0.28	
GFAD, LPJ-GUESS[1]	59 (23 – 359)	13 (6 – 35)	7 (3 – 9)	6 (-2 – 10)	130 (31 – 152)	238 (44 – 238)	39 (12 – 39)	44 (3 – 45)	20 (3 – 20)	Tg C yr^{-1}
LUH2, LPJ-GUESS	115	32	17	14	73	50	16	17	9	
Combined, LPJ-GUESS[2]	135	27	14	10	130	239	39	45	23	
LUH2, LPJ	149	54	23	15	56	39	19	12	12	
LUH2, CABLE	173	61	26	16	23	4	5	5	12	
1991-2000										
Regrowth area, GFAD	1.26	0.98	0.28	0.55	2.96	6.87	2.80	0.92	0.76	M km^2
Regrowth area, LUH2	1.66	0.5	0.21	0.54	2.56	3.30	1.72	0.74	0.30	
GFAD, LPJ-GUESS[1]	70 (23 – 450)	18 (3 – 62)	8 (3 – 14)	8 (0 – 17)	161 (80 – 169)	276 (112 – 276)	33 (8 – 33)	50 (20 – 50)	22 (10 – 22)	Tg C yr^{-1}
LUH2, LPJ-GUESS	130	31	20	17	78	59	21	19	10	
Combined, LPJ-GUESS[2]	147	31	16	11	161	278	33	51	25	
LUH2, LPJ	139	57	23	17	42	35	16	9	12	
LUH2, CABLE	176	73	31	32	29	19	1	4	15	
2001-2010										
Regrowth area, GFAD	3.08	4.99	0.85	0.87	3.60	7.66	3.04	1.18	1.03	M km^2
Regrowth area, LUH2	1.85	0.54	0.22	0.60	2.63	3.45	1.86	0.77	0.31	
GFAD, LPJ-GUESS[1]	-27 (-80 – 375)	-108 (-169 – 347)	-12 (-21 – 50)	13 (0 – 29)	200 (111 – 200)	333 (191 – 333)	55 (29 – 55)	57 (34 – 57)	24 (13 – 34)	Tg C yr^{-1}
LUH2, LPJ-GUESS	155	31	21	19	81	67	25	20	11	
Combined, LPJ-GUESS[2]	58	-96	-4	15	200	333	55	58	25	
LUH2, LPJ	182	64	28	30	66	50	19	11	14	
LUH2, CABLE	234	96	37	39	24	17	6	5	13	

[1] Figures in parentheses are ranges across all sensitivity simulations.

[2] Combined results forced by GFAD and LUH2, as in Fig. 3c.

Table S2. Decadal regrowth forest areas carbon uptake calculations for regrowth forest under full forcing.

	TrBE	TrBD	OTr	TeBE	TeBD	NE	ND	MX	Other	Units
1981-1990										
Regrowth area, GFAD	0.88	0.57	0.19	0.37	2.60	6.37	2.29	0.85	0.66	M km^2
Regrowth area, LUH2	1.48	0.47	0.20	0.49	2.49	3.12	1.62	0.70	0.28	
GFAD, LPJ-GUESS[1]	96 (44 – 542)	26 (14 – 44)	12 (6 – 15)	19 (5 – 23)	209 (90 – 227)	362 (150 – 362)	77 (35 – 77)	72 (28 – 72)	11 (14 – 32)	Tg C yr^{-1}
LUH2, LPJ-GUESS	176	40	25	23	128	107	40	33	15	
Combined, LPJ-GUESS[2]	197	42	21	24	209	364	77	73	34	
LUH2, LPJ	188	61	27	27	66	64	29	14	15	
LUH2, CABLE	360	94	51	59	108	133	48	26	31	
1991-2000										
Regrowth area, GFAD	1.26	0.98	0.28	0.55	2.96	6.87	2.80	0.92	0.76	M km^2
Regrowth area, LUH2	1.66	0.5	0.21	0.54	2.56	3.30	1.72	0.74	0.30	
GFAD, LPJ-GUESS[1]	126 (62 – 687)	52 (30 – 87)	19 (9 – 26)	27 (18 – 37)	255 (173 – 258)	432 (268-432)	75 (46 – 75)	76 (50 – 76)	37 (24 – 38)	Tg C yr^{-1}
LUH2, LPJ-GUESS	215	44	31	29	136	129	42	35	17	
Combined, LPJ-GUESS[2]	238	67	29	31	255	434	75	77	40	
LUH2, LPJ	212	69	29	34	69	64	25	13	17	
LUH2, CABLE	417	121	60	76	137	160	65	32	34	
2001-2010										
Regrowth area, GFAD	3.08	4.99	0.85	0.87	3.60	7.66	3.04	1.18	1.03	M km^2
Regrowth area, LUH2	1.85	0.54	0.22	0.60	2.63	3.45	1.86	0.77	0.31	
GFAD, LPJ-GUESS[1]	89 (21 – 692)	21 (-61 – 449)	13 (2 – 75)	43 (33 – 64)	307 (265 – 307)	549 (420 – 549)	139 (101 – 139)	94 (76 – 94)	47 (38 – 60)	Tg C yr^{-1}
LUH2, LPJ-GUESS	260	43	36	28	145	150	57	44	19	
Combined, LPJ-GUESS[2]	210	35	23	45	307	550	139	95	48	
LUH2, LPJ	264	77	32	36	75	68	30	16	16	
LUH2, CABLE	541	160	74	91	148	187	87	36	35	

[1] Figures in parentheses are ranges across all sensitivity simulations.

[2] Combined results forced by GFAD and LUH2, as in Fig. 3c.

Table S3. Source of information underlying GFAD.

Country	Source	Time Period
United States	US Forest Inventory and Analysis (v5.1) (state summaries)	2000s
Russia	IIASA Russian Forests and Forestry Database	2000s (late)
Canada	Canadian Forest Inventory (state summaries)	2000-2006
Europe	EFISCEN (32 countries)	2000s
China	6th National Forest Inventory	1999-2003
Kazakhstan	National Forest Inventory	2000s
New Zealand	National Forest Inventory	2000s
Mongolia	National Forest Inventory	2000s
Japan	2005 National Forest Inventory	2005
Pan tropics	Saatchi et al. (3)	2000s

Table S4. Mapping of ESA landcover classes to forest types used in this analysis.

Code	Forest class	ESA landcover classes	Additional conditions
TrBE	Tropical broadleaved evergreen	50	latitude ≤ 23°
TrBD	Tropical broadleaved deciduous	60, 61, 62	latitude ≤ 23°
OTr	Other tropical forest	100, 160, 170	latitude ≤ 23°
TeBE	Temperate broadleaved evergreen	50	latitude > 23°
TeBD	Temperate broadleaved deciduous	60, 61, 62	latitude > 23°
NE	Needleleaved evergreen	70, 71, 72	n/a
ND	Needleleaved deciduous	80, 81, 82	n/a
MX	Broadleaved-needleleaved mixed forest	90	n/a
Other	Other forest	100, 160, 170	latitude > 23°

Supporting Figures

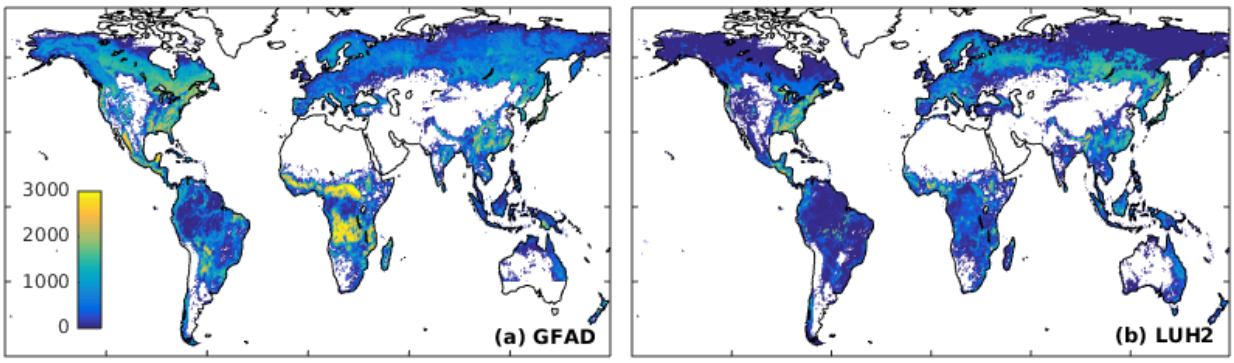

Figure S1. Regrowth forest area (km^2) per 0.5° grid cell based on GFAD (a) and LUH2 (b). Note that the total forest area is constrained by ESA CCI forest cover (see Methods). All cells containing at least 1% forest cover are shown here.

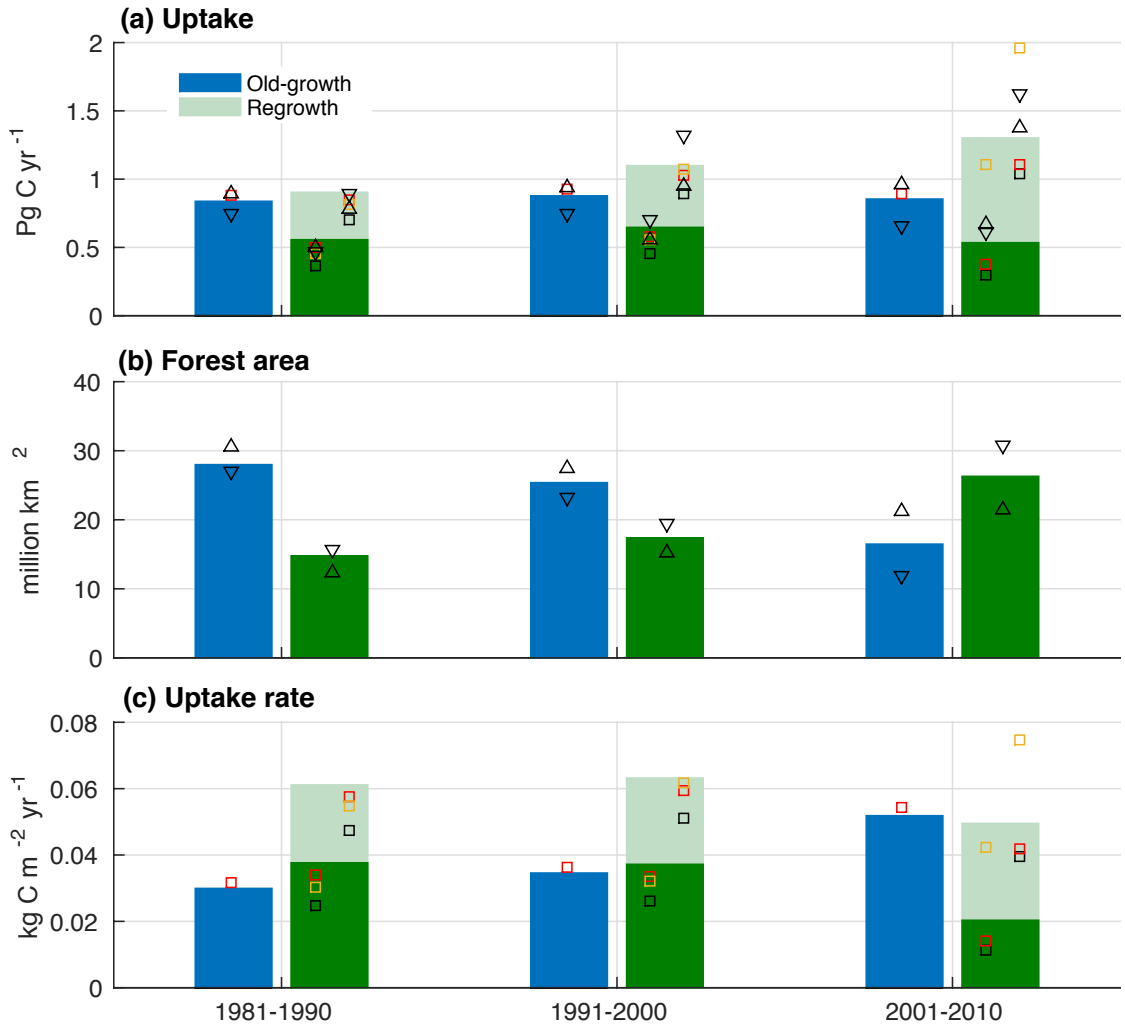

Figure S2. Total carbon uptake (a), forest area (b) and uptake rate (c), split by old-growth and regrowth forest for the three decades preceding 2010. Sensitivity studies are shown as for Fig. 2. Note that the primary forest area in 1981-1990 and 1991-2000 may be slightly overestimated because the base time period for the stand age data is 2001-2010 and we have no information for the age of stands in e.g. 1990 if the most recent reestablishment was post 1990. In the absence of information about the age of these forest fractions in 1990 and 2000, the fractions are assigned to old-growth forest, whereas in reality some of it might have been regrowth forest or agricultural land. Following from this, for 1981-1990 and 1991-2000, the upper and lower sensitivities for forest stand age both result in a regrowth forest area that falls below the central estimate - the lower bound of stand age results in more forest being classified as very young in 2010, and thus being assigned to old-growth forest during the earlier decades. The substantially lower uptake rate of regrowth forest during 2001-2010 is due to a large establishment of regrowth forest in the tropics during this decade, resulting in net emission in much of this region (Fig. S3). Uptake is maintained in the event that the previous land-use was cropland (orange squares) due to the recovery of carbon-depleted cropland soils.

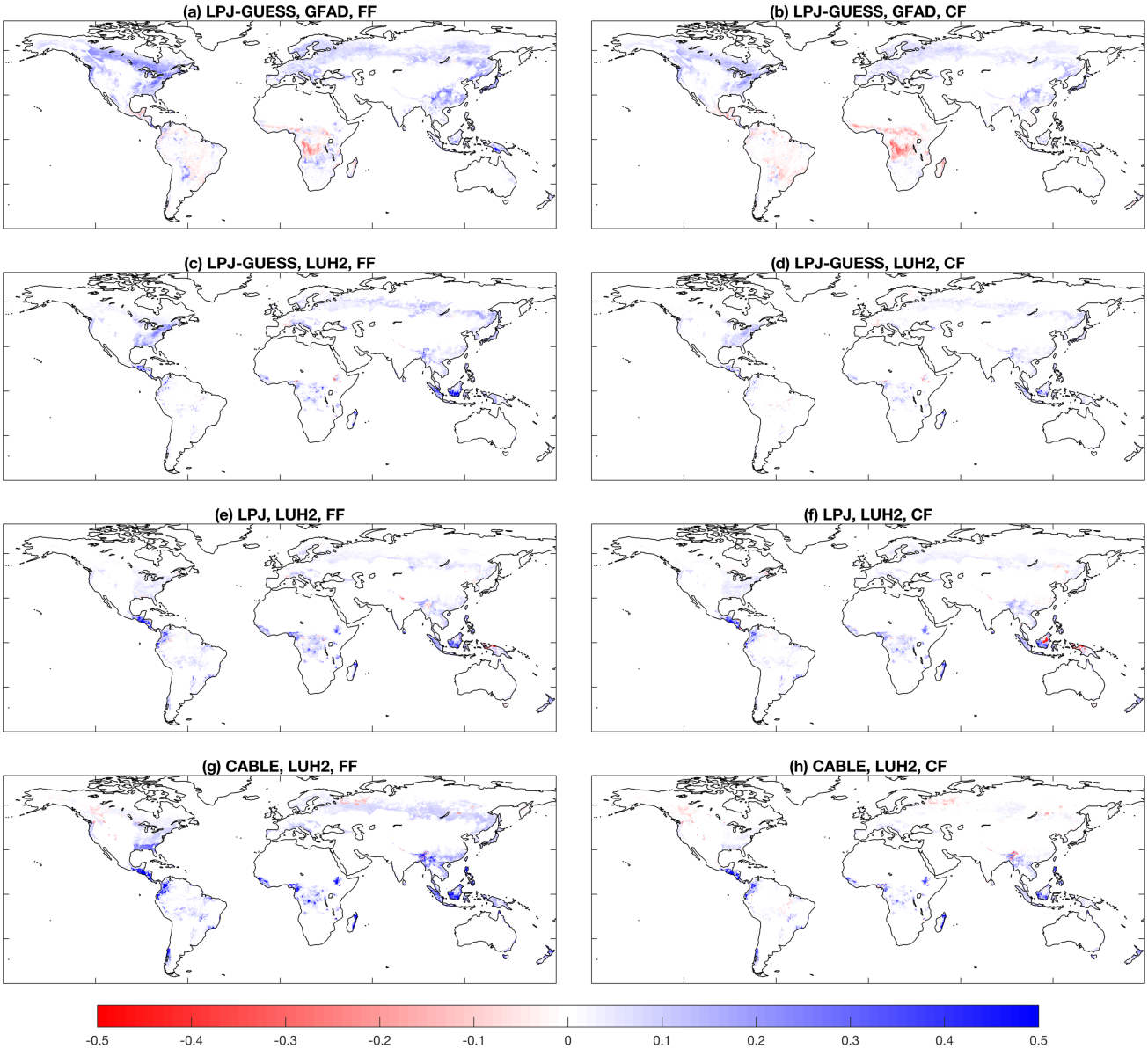

Figure S3. Maps of carbon uptake in regrowth forests (kg C m^{-2} yr^{-1}, 2001-2010 mean) as simulated by the model and forcing dataset combinations in this study. Blue shows carbon uptake and red carbon loss. Left column shows results with full environmental forcing and right column results with fixed pre-industrial forcing.

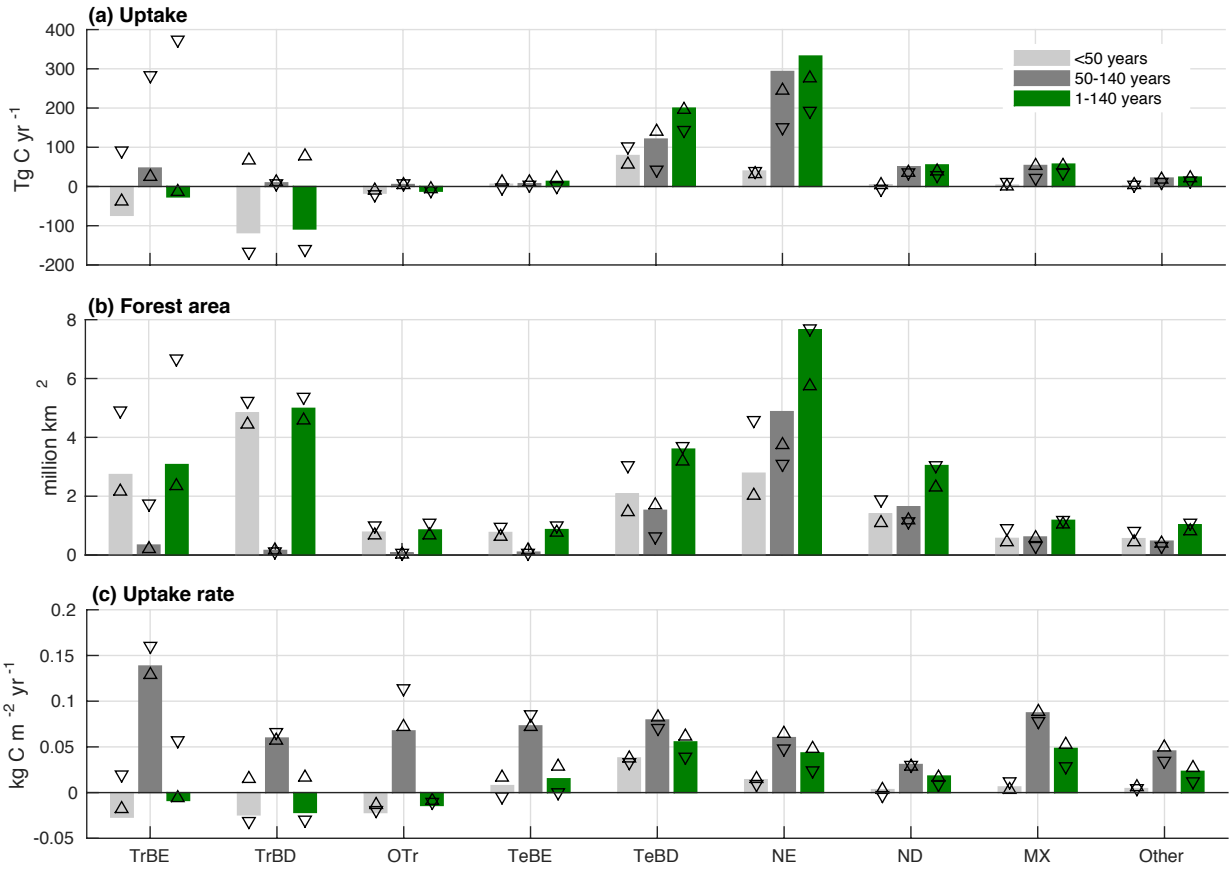

Figure S4. Contribution to regrowth sink by regrowth stand age in the CF simulation of LPJ-GUESS forced by GFAD for 2001-2010. Light grey bars show results for regrowth stands less than 50 years old, dark grey bars for stands between 50 and 140 years old, and green bars the total over 1-140 years. (a) Carbon uptake. (b) Forest area. (c) Uptake rate calculated by dividing carbon uptake by forest area for each forest type. Symbols show results from sensitivity simulations as in Fig. 2. Uncertainty becomes large for the tropical regrowth forest because much of the regrowth forest in the tropics is very young. Older regrowth stands show a pattern of carbon uptake rate that follows the relative productivity of these different forest types, whilst younger regrowth stands tend to have much lower net carbon uptake as a result of larger soil legacy fluxes and a greater fraction of stands without canopy closure.

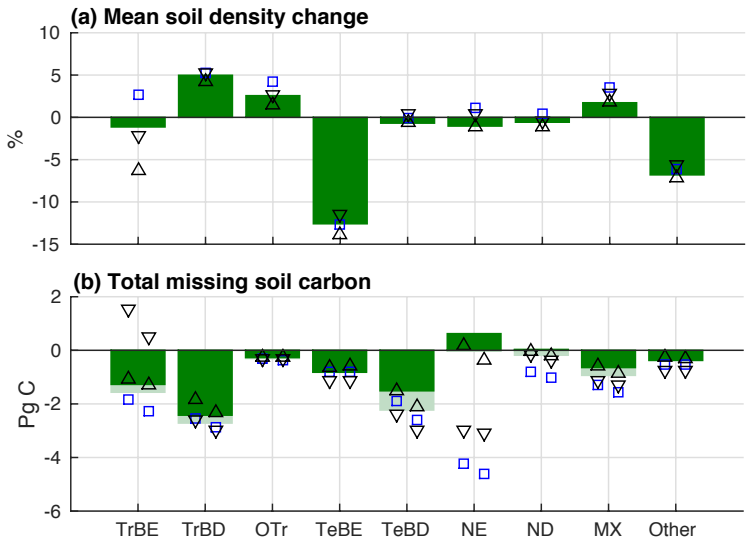

Figure S5. As for Fig. 4, but for soil and litter carbon. Note that CF and FF simulations give virtually identical results in panel a.

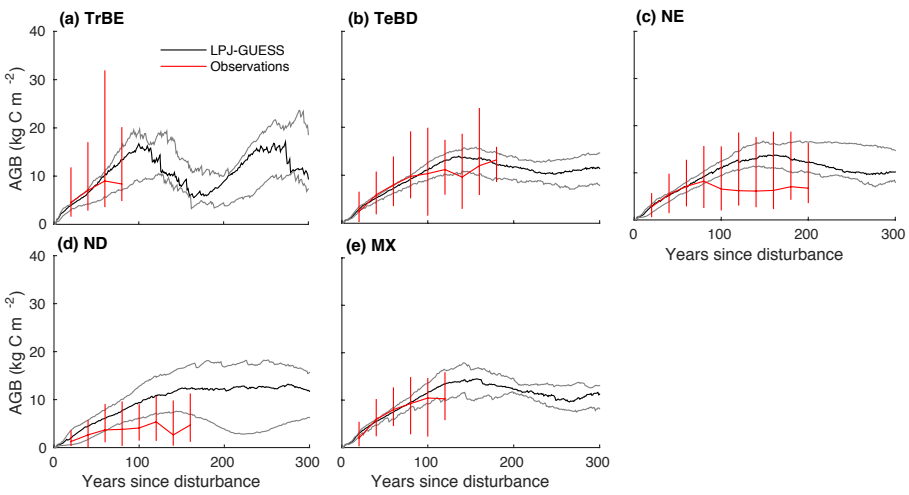

Figure S6. Comparison of biomass regrowth trajectories calculated with LPJ-GUESS with observations. The red lines are median above-ground biomass (AGB) for 20 year age bins, taken from Teobaldelli et al. (17) and Poorter et al. (18, 19) for locations within the area of that forest type. Only bins with at least 20 observations are plotted (insufficient data for TrBD and TeBE). Error bars show the 10th and 90th percentiles of the data. The median of LPJ-GUESS results for simulations at the same locations is plotted as a black line with 10th and 90th percentiles in grey. A single 0.5° x 0.5° grid cell may be represented multiple times in the average if there are multiple observations located within that cell. The simulation was 300 years under recycled, detrended, 1986-2015 climate (forcing dataset as in main text) and a fixed 2015 atmospheric CO_2 mixing ratio of 401 ppm, to be appropriate for current conditions. Directly after spin-up, all grid cells were subject to stand-clearing disturbances for all patches. The vegetation was then allowed to regrow without being subject to further stand-replacing disturbances. Simulated AGB was calculated as 0.75 multiplied by the simulated total vegetation biomass to account for the below-ground fraction (20).

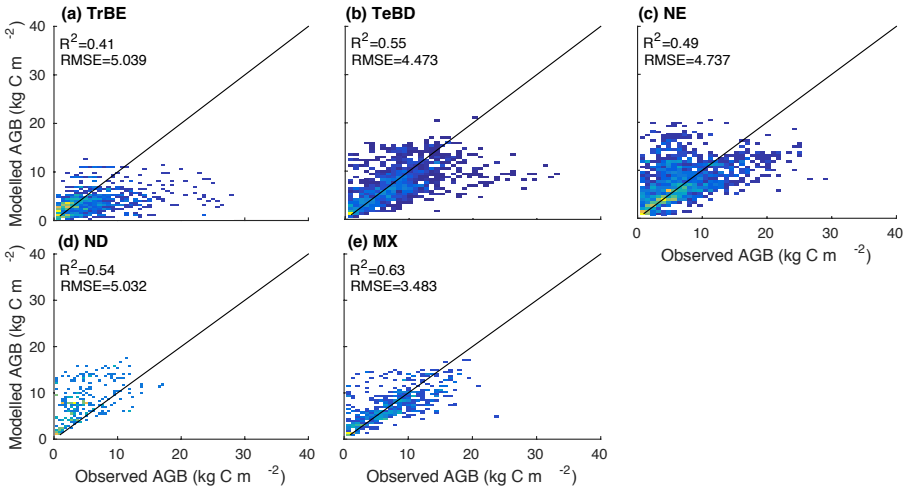

Figure S7. Comparison of observed and LPJ-GUESS simulated AGB for different forest types. Each point represents one biomass observation and age, plotted against the biomass simulated for the corresponding stand age by LPJ-GUESS. Data and simulations as described in Fig. S6. Brighter colors indicate a higher density of points.

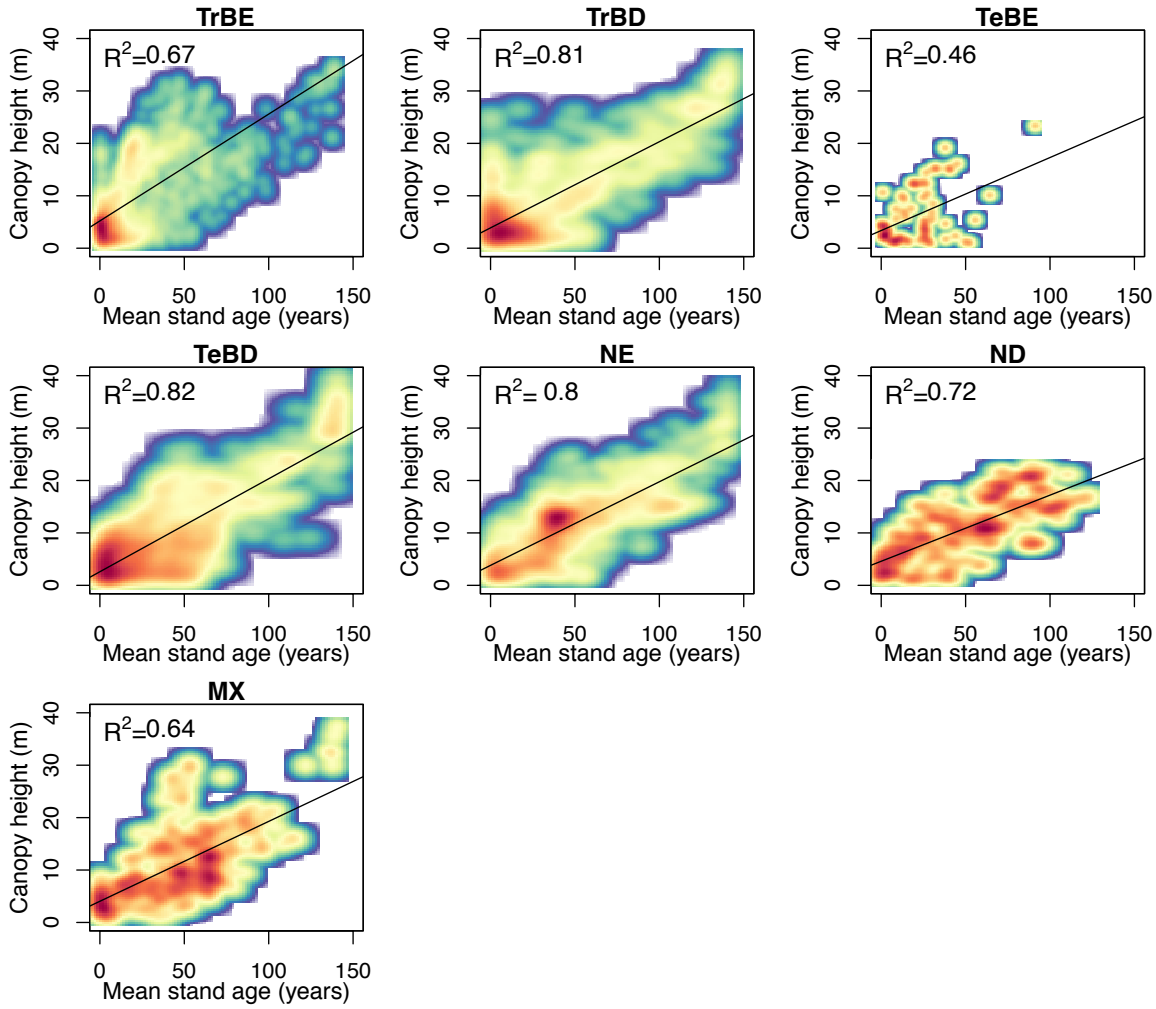

Figure S8. Relationship between GFAD mean stand age at 0.5° and mean canopy height as given by Simard et al. (21). Brighter colors indicate a higher density of points. Black lines show the best fit linear regression.

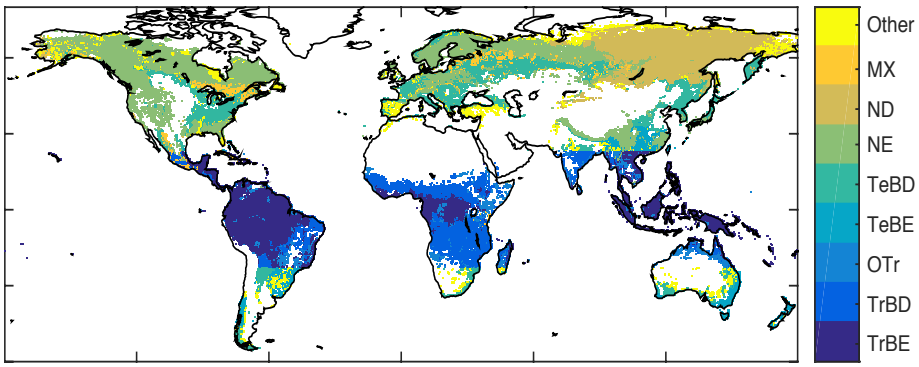

Figure S9. Locations of forest types. Only grid cells with at least 5% area classified as forest are shown for clarity.

Supporting Data

Dataset S1

ESA_forest_cover_regrowth_analysis.txt

- Raster file containing fraction forest cover per grid cell as used in this analysis.
- -99 is no data

Dataset S2

ESA_forest_9regions_regrowth_analysis.txt

- Raster file containing dominant forest type per grid cell as used in this analysis.
- Codes: 1 TrBE, 2 TrBD, 3 OTr, 4 TeBE, 5 TeBD, 6 NE, 7 ND, 8 MX, 9 Other
- -99 is no data

Supporting References

1. Poulter B, et al. (2018) *The global forest age dataset (GFADv1.0), link to NetCDF file* Available at: https://doi.pangaea.de/10.1594/PANGAEA.889943.
2. Pollard JE, et al. (2006) *Forest Inventory and Analysis National Data Quality Assessment Report for 2000 to 2003.* Available at: http://www.fs.fed.us/rm/pubs/rmrs_gtr181.pdf.
3. Saatchi SS, et al. (2011) Benchmark map of forest carbon stocks in tropical regions across three continents. *Proc Natl Acad Sci* 108:9899–9904.
4. Espírito-Santo FDB, et al. (2014) Size and frequency of natural forest disturbances and the Amazon forest carbon balance. *Nat Commun* 5:3434.
5. Cole LES, Bhagwat SA, Willis KJ (2014) Recovery and resilience of tropical forests after disturbance. *Nat Commun* 5:3906.
6. Thonicke K, Venevsky S, Sitch S, Cramer W (2001) The role of fire disturbance for global vegetation dynamics: coupling fire into a Dynamic Global Vegetation Model. *Glob Ecol Biogeogr* 10(6):661–677.
7. Ellis EC, Goldewijk KK, Siebert S, Lightman D, Ramankutty N (2010) Anthropogenic transformation of the biomes, 1700 to 2000. *Glob Ecol Biogeogr* 19(5):589–606.
8. Krause A, Pugh TAM, Bayer AD, Lindeskog M, Arneth A (2016) Impacts of land-use history on the recovery of ecosystems after agricultural abandonment. *Earth Syst Dyn* 7:745–766.
9. Guo L, Gifford R (2002) Soil carbon stocks and land use change: a meta analysis. *Glob Chang Biol* 8:345–360.
10. Nyawira SS, Nabel JEMS, Don A, Brovkin V, Pongratz J (2016) Soil carbon response to land-use change: evaluation of a global vegetation model using observational meta-analyses. *Biogeosciences* 13(19):5661–5675.
11. Olin S, et al. (2015) Soil carbon management in large-scale Earth system modelling : implications for crop yields and nitrogen. *Earth Syst Dyn* 6:745–768.
12. Sitch S, et al. (2003) Evaluation of ecosystem dynamics, plant geography and terrestrial carbon cycling in the LPJ dynamic global vegetation model. *Glob Chang Biol* 9:161–185.
13. Haverd V, et al. (2013) A stand-alone tree demography and landscape structure module for Earth system models. *Geophys Res Lett* 40(19):5234–5239.
14. Haverd V, Smith B, Nieradzik LP, Briggs PR (2014) A stand-alone tree demography and landscape structure module for Earth system models: Integration with inventory data from temperate and boreal forests. *Biogeosciences* 11:4039–4055.
15. Hansis E, Davis SJ, Pongratz J (2015) Relevance of methodological choices for accounting of land use change carbon fluxes. *Global Biogeochem Cycles* 29:1230–1246.
16. Chazdon RL, et al. (2016) Carbon sequestration potential of second-growth forest regeneration in the Latin American tropics. *Sci Adv* 2:e1501639.
17. Teobaldelli M, Somogyi Z, Migliavacca M, Usoltsev VA (2009) Forest Ecology and Management Generalized functions of biomass expansion factors for conifers and broadleaved by stand age,

growing stock and site index. *For Ecol Manage* 257:1004–1013.
18. Poorter L, et al. (2016) Biomass resilience of Neotropical secondary forests. *Nature* 530(7589):211–214.
19. Poorter L, et al. (2016) Data from: Biomass resilience of Neotropical secondary forests. Nature. *DRYAD*. doi:10.5061/dryad.82vr4.
20. Penman J, et al. (2003) *Good Practice Guidance for Land Use, Land-Use Change and Forestry* (Kanagawa, Japan).
21. Simard M, Pinto N, Fisher JB, Baccini A (2011) Mapping forest canopy height globally with spaceborne lidar. *J Geophys Res* 116:G04021.